RSC Advances

ROYAL SOCIETY OF CHEMISTRY

www.rsc.org/advances

Anti-biofilm property of magnesium metal via alkaline pH

Hui Qin[#], Yaochao Zhao[#], Mengqi Cheng, Qi Wang, Qiaojie Wang, Jiaxing Wang,

Yao Jiang*, Zhiquan An*, Xianlong Zhang*

Department of Orthopedics, Shanghai Sixth People's Hospital, Shanghai Jiao Tong University, Shanghai 200233, China

[#] These authors contributed equally to this work

* Corresponding authors:

Jiang Yao -Tel: +86 21 6436 9183; Fax: +86 21 6470 1363; Electronic mail: jiangyao197826@163.com

Xianlong Zhang -Tel: +86 21 6436 9184; Fax: +86 21 6470 1363; Electronic mail: zhangxianl197826@163.com

Zhiquan An -Tel: +86 21 6436 9184; Fax: +86 21 6470 1363; Electronic mail: anzhiquan197826@163.com

1

Table of contents entry

Against bacterial growth

No antibacterial effect

biofilm

$$Mg+2H_2O \longrightarrow Mg^{2+}+2OH^-+H_2$$

OH⁻
Mg²⁺
bacteria
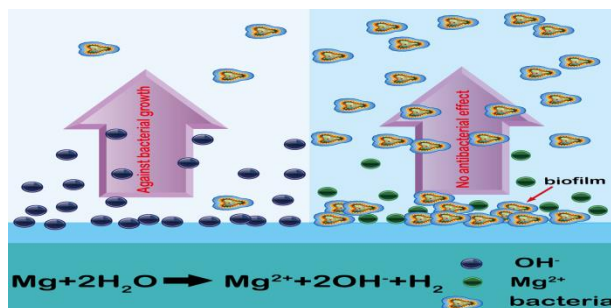
Mg prevents bacteria biofilm formation via high alkalinity at its surface rather than by high Mg ion concentration.

Abstract

Prevention of implant-associated infection (IAI) by inhibiting biofilm formation on implant is crucial to orthopedic surgery. In this work, the anti-biofilm activity of magnesium (Mg) is assessed using *Pseudomonas aeruginosa* (*P. aeruginosa*) and *Staphylococcus epidermidis* (*S. epidermidis*), two biofilm producing strains, *in vitro*, and using *S. epidermidis in vivo*. The effects of high Mg^{2+} concentration and alkaline pH on biofilm are evaluated in two separate experiments *in vitro*. Mg shows biofilm resistance proportionally to the degradation of Mg *in vitro*, which is better than that of the corresponding alkaline pH, and high Mg^{2+} concentration has no such effect. Microbiological cultures and histological results demonstrate the ability of Mg against bacterial infection to reduce the risk of IAI *in vivo*. The results demonstrate that Mg prevents bacteria biofilm formation by high alkalinity at its surface rather than by high Mg^{2+} concentration, thus providing a promising new strategy for combating IAI.

1. Introduction

Insertion of implants in the body to repair bone diseases, such as bone fracture or bone defect, will unavoidably disturb the adjacent tissues and the microcirculation, so bacteria contaminated in surgery may escape from the host defense systems. The bacteria adhere to and grow on the surfaces of implants, then synthesize a complex glycocalyx and form biofilm,[1-3] which would protect bacteria from antibiotic treatment and immune cell surveillance,[4-5] leading to implant-associated infection (IAI). Once IAI occurs, the patients have to receive implants removal, multiple debridement surgeries and prolonged periods of antibiotic therapy. These will result in extreme and unnecessary suffering even disability,[6] and the incurred average revision costs was estimated to be greater than $100,000 per an infected case.[7] In some cases, IAI persists despite treatment,[8]   so prevention of IAI is very important. For biofilm formation is the key to IAI, developing new strategies that prevent biofilm formation are urgently needed in the orthopedic community.

Magnesium (Mg) has been proved to have unique properties: low elastic modulus close to that of nature bone minimize stress shielding effects,[9] biodegradability avoid the need for a second surgical operation for implant removal,[10-11] good mechanical strength make them be more suitable for load-bearing applications than bio-absorbable polymers,[11-12] which make it become a new implant material for

orthopedic applications to replace stainless steels, titanium (Ti) and Ti alloys, absorbable polymers used now. In the last few years, Robinson et al. proved that Mg can reduce the growth of bacteria in Mueller–Hinton broth.[13] Lock et al. verified that the bacterial multiplication in artificial urine is inhibited by Mg.[14-15] They believed that Mg is a promising biomaterial to prevent infection. However, detection of bacteria growth on Mg surface was ignored. Obviously, bacterial adhesion, growth and eventually biofilm formation are essential to IAI. Thus the anti-biofilm property of Mg needs further explorations.

Accordingly, in this study, two different biofilm-producing bacteria: *Pseudomonas aeruginosa* (*P. aeruginosa* ATCC 27853) (Gram-negative), and *Staphylococcus epidermidis* (*S. epidermidis* ATCC 35984) (Gram-positive) were chosen to evaluated the anti-biofilm effect of Mg *in vitro*. And *S. epidermidis* was chosen to evaluate it *in vivo*.

2. Materials and methods

2.1. Sample preparation and characterization

5

For *in vitro* experiments, purity Mg and pure titanium (Ti) were fabricated into 10 mm square plates with a thickness of 2 mm. For *in vivo* experiments, the above materials were formed into 150 mm long, 1.2mm in diameter short Kirschner wires. The above samples were polished up to 2000 grid, and ultrasonically cleaned in acetone and alcohol for 10 min, respectively, for later experiments.

The samples were examined by scanning electron microscopy (SEM; Joel JSM-6310LV, Japan) coupled with energy-dispersive X-ray spectroscopy (EDS; EDAX Si/Li detector) analysis to show the surface morphology and elemental composition before experiment.

2.2. Bacteria preparation and characterization

P. aeruginosa (ATCC 27853) and *S. epidermidis* (ATCC 35984) were obtained in a freeze-dried form from the American Type Culture Collection (Rockefeller, MD). Pure cultures of above strains were aerobically cultured for 24 h at $37^{o}C$ on sheep blood agar (SBA) plates. A single colony of each of the pure cultures was collected and incubated in 6 ml of sterile Trypticase Soy Broth (TSB; BD Biosciences, Franklin Lakes, NJ) at $37^{o}C$ with agitation at 220 rpm for 12 h. The inocula of the strains were prepared through adjusting the concentration of bacterial broth culture to 1×10^{8} colony forming units (CFUs)/ml in TSB as determined by McFarland, then diluting to

1×10^6 CFUs/ml with Dulbecco's modified Eagle's medium (DMEM, Gibco^{TM}, Invitrogen), supplemented with 10% fetal bovine serum (FBS, Hyclone) for simulating physiological environment. For *in vivo*, *S. epidermidis* was prepared at a concentration of 1×10^5 CFUs /ml in phosphate-buffered saline solution (PBS).

2.3. Mg corrosion in medium

3ml DMEM supplemented with 10% FBS or prepared bacteria suspension (1×10^6 CFUs/ml) was added to each well in 12-well plate contained samples, and incubated at 37°C for 1, 3, or 5 days. At each time point, the medium were centrifugalized at 10000 g for 3 min to remove the insoluble corrosion products and bacteria. The pH of medium was measured using a pre-calibrated pH meter (Mettler Toledo). The Mg ion (Mg^{2+}) concentration in the solutions was determined using inductively coupled plasma-atomic emission spectroscopy (ICP-AES; Perkin Elmer Optima 2000 DV).

After removing from the medium, the Mg samples were ultrasonic vibrated (150 W) in 5ml PBS for 5 min at 50 Hz to detach the adherent bacteria, then dried overnight at room temperature, cleaned by 200 g/l chromic acid to remove the corrosion products and weighed. The samples were weighed before and after immersion in the medium to determine the sample degradation. The corrosion rate was calculated by the following equation: $C = (M_0-M_x)/\rho At$ (M_0 is the initial mass and M_x is the mass at the respective

7

time points, ρ is the density of Mg, A is the initial sample surface area and t is the

immersion time).

2.4. *In vitro* anti-biofilm effect

3ml prepared bacteria suspension (1×10^6 CFUs/ml) was added to each well in 12-well

plate contained samples, and incubated at 37^oC for 1, 3, or 5 days. At each time point,

the planktonic bacteria in the culture medium were analyzed by the spread plate

method; the adherent bacteria on the samples' surface were determined by the spread

plate method, confocal laser scanning microscopy (CLSM) and SEM.

2.4.1. Anti-biofilm assay by the spread plate method

At each time point, the culture medium was collected to determine the viable counts

of planktonic bacteria. For assessing the number of viable adherent bacteria, the

samples were gently washed with PBS three times to remove loosely adherent

bacteria from the samples surface, the adhered bacteria on each specimen were

detached into 1 ml of PBS by ultrasonic shaking (150 W) 5 min at 50 Hz, then the

resulting bacterial suspension was used to count the viable bacteria adhered on the

specimens. The above solutions were serially diluted 10-fold, plated in triplicate onto

SBA and incubated at 37^oC for 24 h. The number of CFUs on the SBA was counted in

accordance with the National Standard of China GB/T 4789.2 protocol. The antibacterial rates with regard to planktonic bacteria in the culture medium and the antibacterial rates for adhered bacteria on the specimens were calculated based on the following formulas: (1) Antibacterial rate for planktonic bacteria in the medium (Rp) (%)=(B-A)/B×100% and (2) Antibacterial rate for adherent bacteria on the specimen (Ra) (%)=(D-C)/D×100%. Here, A indicates the average number of viable bacteria in the culture medium inoculated with the specimen, B is the average number of viable bacteria in the culture medium inoculated without specimen (blank control), C is the average number of viable bacteria on the Mg specimens, and D is the average number of viable bacteria on the Ti.

2.4.2. Anti-biofilm assay by CLSM

After rinsed with PBS three times, the samples were placed into a new 24-well plate and stained with 500μl combination dye (LIVE/DEAD BacLight bacteria viability kits, Invitrogen) for 15 min, and analyzed with a confocal laser scanning microscope (LSM 510 meta; Zeiss, Germany) since the viable bacteria with intact cell membrane stain green, whereas nonviable bacteria with damaged membranes stain red.

2.4.3. Anti-biofilm assay by SEM

After rinsed with PBS three times, the samples were fixed with 2.5% glutaraldehyde solution for 4 hours, then dehydrated in the graded ethanol series (30, 50, 70, 80, and 90 v/v%) for 12 min each sequentially, with the final dehydration conducted in absolute ethanol (twice), freeze dried, coated with platinum, and observed using a SEM.

2.5. Effect of Mg ion on growth of bacteria *in vitro*

Medium with Mg^{2+} concentration at the highest concentration determined by the above Mg corrosion test (18mg/dl) by adding $MgCl_2$ to DMEM with 10% FBS was prepared. 3ml prepared bacteria suspension (1×10^6 CFUs/ml) with Mg^{2+} concentration at 18mg/dl was added to each well in 12-well plate contained Ti samples, and incubated at 37°C for 1, 3, or 5 days. The effect of Mg^{2+} on bacteria was assessed by the spread plate method. The formulas are same as above, but here, A indicates the average number of viable bacteria in the culture medium with higher Mg^{2+} concentration (18mg/dl), B is that in the culture medium with normal Mg^{2+} concentration (2.11 mg/dl, determined by ICP-AES); C is the average number of viable bacteria on the Ti with higher Mg^{2+} concentration, and D is that on the Ti with normal Mg^{2+} concentration.

2.6. Effect of pH on growth of bacteria *in vitro*

Media with different pH (8, 9, 10) by adding 1 N NaOH to DMEM with 10% FBS were prepared. 3ml prepared bacteria suspension (1×10^6 CFUs/ml) with different pH was added to each well in 12-well plate contained Ti samples, and incubated at 37^oC for 1, 3, or 5 days. The effect of pH on bacteria was assessed by the spread plate method. In this test, A indicates the average number of viable bacteria in the culture medium with different pH, B is that in the culture medium without adding NaOH; C is the average number of viable bacteria on the Ti with different pH, and D is that on the Ti without adding NaOH.

2.7. *In vivo* anti-biofilm effect

2.7.1. Implant-related femur osteomyelitis model in rats

The experimental protocol was approved by the Animal Care and Experiment Committee of Sixth Peoples Hospital affiliated to Shanghai Jiao Tong University, School of Medicine, and the experiment was performed in compliance with the relevant laws and institutional guidelines of China. Forty male Sprague Dawley rats 3 months in age and weighing an average of 200 g (160-235g) were used. *S.*

epidermidis (ATCC 35984) in a concentration of 1×10^5 CFUs/ml was used to create bone infection. Surgery was performed under general anesthesia by weight-adopted intraperitoneal injection of 4% chloral hydrate (0.9ml/100g body wt). After the left leg of rat shaved and disinfected with povidone iodine, the knee was opened via a medial parapatellar incision. Followed patellar dislocation and exposure of the femoral condyles, the femoral medullary cavity was opened at the middle of femoral trochlear and widened gradually with Kirschner wires up to a diameter of 1.5 mm. After removal, 10μl of either PBS or PBS containing ATCC 35984 in a concentration of 1×10^5 CFUs/ml was injected into the medullary cavity. Then a Mg or Ti Kirschner wire (diameter: 1.2 mm) was inserted. According to the study groups, four groups (Table 1) were investigated. After the opening in the femoral trochlear sealed with bone wax, the surgical site was irrigated with sterile saline and the soft tissues and skin were closed. Following surgery, the animals were housed in separate cages and allowed to eat and drink ad libitum. Weight bearing was started immediately postoperatively, and the animals were monitored daily. Buprenorphine was administered for 2 days as an analgesic, but no antibiotic was administered.

Table 1. Details of Animal Experiments.

Group	Number(n)	Implant	Inoculation
I	10	Ti wire	*S. epidermidis* 10^3 CFUs/10μl
II	10	Mg wire	*S. epidermidis* 10^3 CFUs/10μl

| III | 10 | Ti wire | PBS/10µl | |
| IV | 10 | No | *S. epidermidis* 10^3 CFUs/10µl | |

2.7.2. Radiographic and micro-computed tomography scanning

At 0, 2, 4 weeks post-surgery, lateral radiographs of femur were obtained. All the radiographic images were assessed by three independent observers in a blind manner according to the literature,[16] including osteolysis, periosteal reaction and general impression.

2.7.3. Microbiological evaluation

After 28 days, the animals were sacrificed and the operated femurs were aseptically retrieved. The implant wires were aseptically explanted and rolled over SBA for semi-quantifying bacteria adhesion on the implant wires. Then they were placed in 4ml PBS, for quantifying bacteria adhesion, sonicated and vortexed to dislodge adhered bacteria. Using the spread plate method mentioned above, the adhered bacteria were counted.

Randomly five femurs of every group were snap frozen and milled to a powder under sterile conditions.[17] Then the bone powder of one femur was agitated in 2ml PBS for 3 min. After centrifuging at 10,000g for 15 sec, the supernatant was withdrawn for serial (10-fold) dilutions. The samples were analyzed for CFUs/femur using the spread plate method

2.7.4. Histological evaluation

The remaining five femurs of each group were fixed in 10% neutral buffered formalin for 48 h, then decalcified using 10% EDTA solution (pH 7.4) for 14 days, and dehydrated in inclining alcohol solution, embedded in paraffin. 5-mm transverse sections of each specimen were collected. Hematoxylin and eosin (HE) staining was implemented to examine the morphology, and Giemsa staining was used to assess bacterial contamination.

2.8. Statistical analysis

The experiments were conducted in triplicate and repeated three times. SPSS 18 program was used to perform statistical analysis. The data were expressed as the means ± standard deviations. The one way ANOVA and Student-Newman-Keuls post

14

hoc tests were used to determine the level of significance and p values less than 0.05

was considered to be statistically significant.
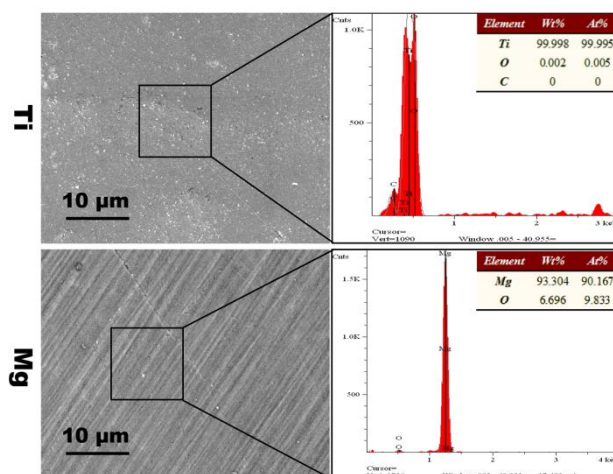
3. Results

3.1. Material characterizations

Figure 1. Surface morphology of the Ti and Mg surface examined by SEM. The areas

where the EDS analysis took place are indicated in the corresponding SEM images.

The surface microstructures and elemental composition of the samples are shown in

Figure 1. Ti surface shows uniform dot scratches, while Mg surface appears even strip

scratches. Apart from oxygen, no other impurities are detected in the two materials.

15

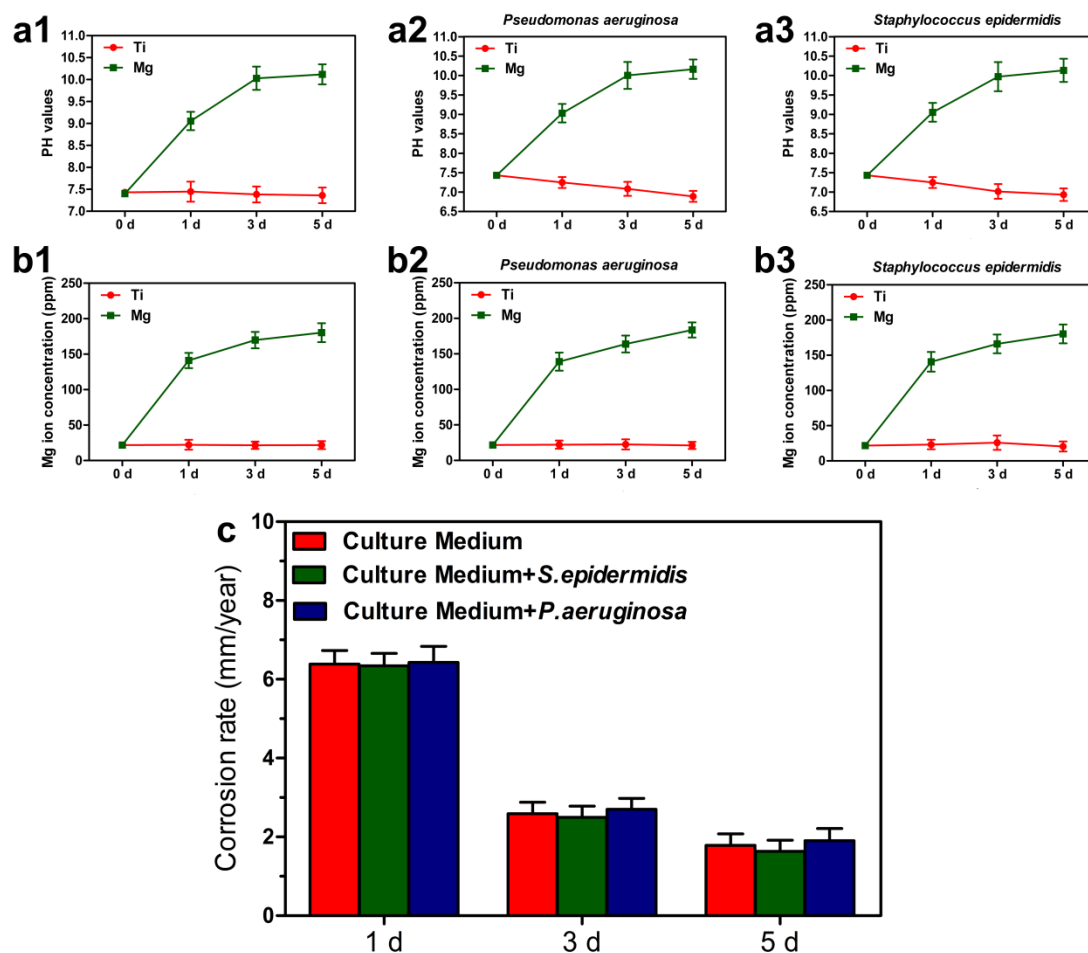## 3.2. Mg degradation in medium

Figure 2. Mg corrosion in the medium with or without bacteria. pH (a), Mg^{2+} concentration (b) and corrosion rate (c) after samples soaking in the medium (a1, b1), the medium with *P. aeruginosa* (a2, b2), the medium with *S. epidermidis* (a3, b3) for 1, 3 and 5 days.

The pH value of the medium cultured with Mg without bacteria rapidly rises over the first day to an average of 9.06 and then slowly increases to 10.03 and 10.12 at day 3

and day 5 (Figure 2a-1), the concentration of Mg^{2+} surges within the first 1 day from

2.11 mg/dl (the normal Mg^{2+} concentration in the medium) to an average of 14.10

mg/dl and then slowly increases to 16.98 mg/dl and 18.03 mg/dl at day 3 and day 5

(Figure 2b-1). As microbial adhesion, metabolism may impact on the degradation of

Mg, the effect of bacteria on corrosion of Mg is accessed. As shown in the Figure.

2a-2, 2a-3, 2b-2, 2b-3, the pH value in the medium with *P. aeruginosa* is 9.03, 10,

10.16, with *S. epidermidis* is 9.05, 9.97, 10.13 at day 1, 3, 5; the corresponding

concentration of Mg^{2+} is 13.9, 16.38, 18.37 mg/dl for *P. aeruginosa*, and 14.07, 16.62,

18.03 mg/dl for *S. epidermidis*, which are almost the same as those in the medium

without bacteria. The corrosion rate is shown in Figure. 2c, no significant difference

can be detected from the corrosion rate of Mg with and without bacteria in the

medium at three time points. These results indicate that the bacteria had little effect on

the degradation of Mg.

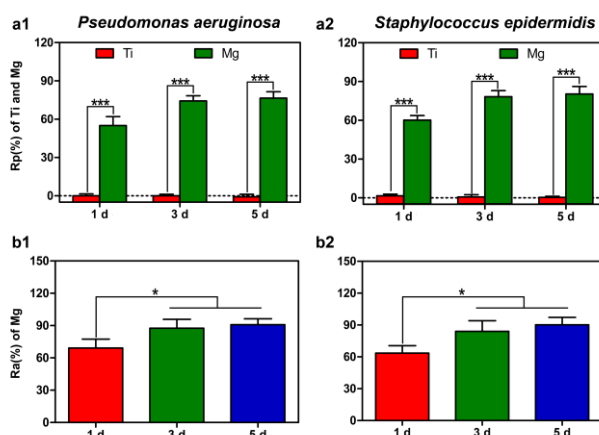### 3.3. *In vitro* anti-biofilm property

Figure 3. Biofilm formation on Ti and Mg surfaces examined by the spread plate method. Rp values were used to estimate the amount of living bacteria in the medium (a1, a2). Ra values were used to estimate the amount of living bacteria on Ti or Mg surface (b1, b2). $^{*}p < 0.05$, $^{***}p < 0.001$.

The antibacterial effects against planktonic bacteria in the medium (Rp) and against adherent bacteria on the specimens (Ra) at day 1, 3 and 5 are evaluated, and the results are shown in Figure 3. The Ti specimens have an Rp value of about 0% for two microorganisms at all three time points. Compared to Ti, the Mg samples have the higher Rp value of 55.1%, 74.3% and 76.5% at day 1, 3, 5 for *P. aeruginosa*, 60.2%, 78.3% and 80.4% for *S. epidermidis*, respectively (Figure 3a-1, 3a-2). Compare with the antibacterial effects against planktonic bacteria, Mg is more effective in preventing bacteria colonization on the specimens. The Ra value of Mg is 69.1%, 87.5% and 90.9% at day 1, 3, 5 for *P. aeruginosa*, 63.5%, 84% and 90.2% for *S. epidermidis* (Figure 3b-1, 3b-2).
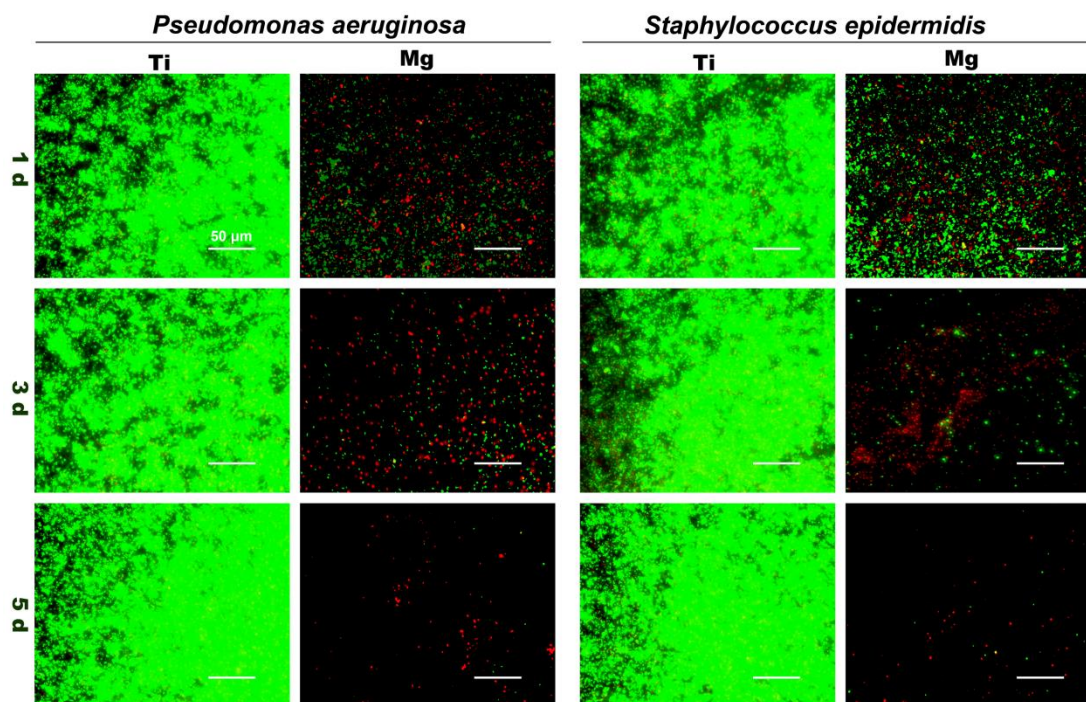
Figure 4. Fluorescent images of biofilm formation on Ti and Mg surface at day 1, 3 and 5 obtained by CLSM after staining with the Baclight dead/live stain. Magnification, ×400. The scale bar is 50μm.

The ability of the Mg to prevent bacteria colonization and biofilm formation is also verified by CLSM and SEM observations. The CLSM views of bacteria colonization is shown in Figure 4. At day 1, 3, 5, an intense green fluorescence on the surface of Ti samples can be observed, which indicates lots of bacteria adhesion, better viability and significant biofilm formation, A less green intense fluorescence and more red fluorescence were found on the surfaces of Mg at day 1, which indicates a less amount of bacteria adhesion, a higher proportion of bacterial death and a low level of

19

biofilm formation. The live bacterial colonies were sparsely distributed on the surface

of Mg at day 3 and became lesser at day 5, which indicates few bacteria adhesion,
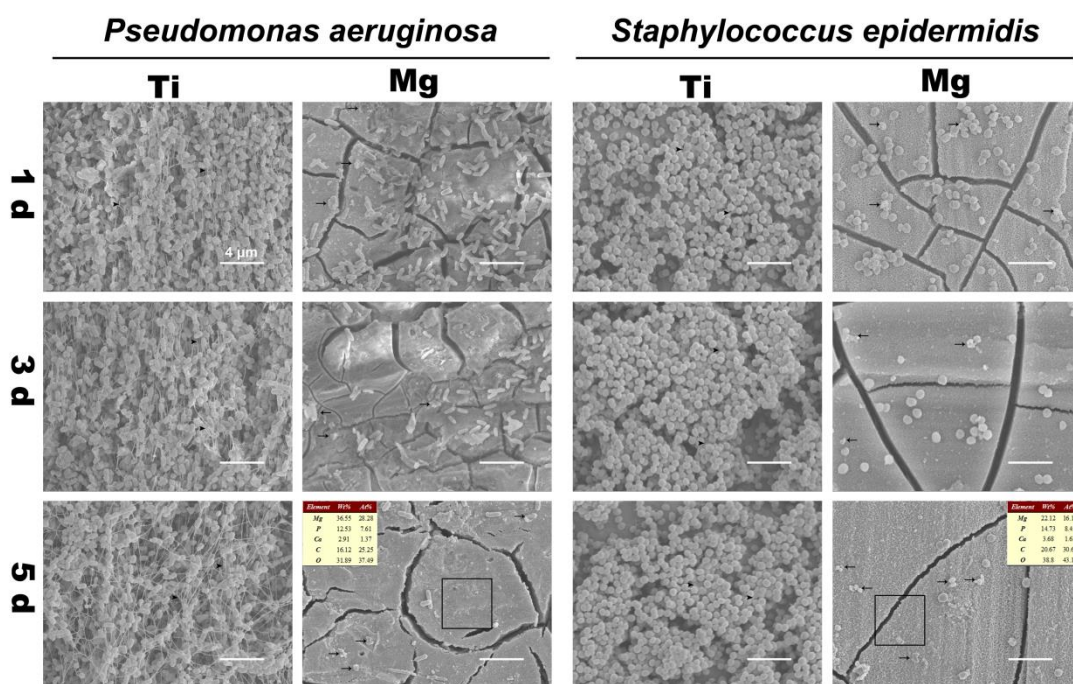
survival and no biofilm formation.

Figure 5. SEM morphology of biofilm formation on Ti and Mg surface at day 1, 3

and 5. The inset shows the EDS result of a typical corroded area of Mg at day 5.

Magnification, ×5000. The scale bar is 4μm. Arrowhead and arrow mark the

filamentous structure among bacteria in biofilm, and the ruptured, lysed cell,

respectively.

Similar trend is observed by SEM. As shown in Figure 5, the large amount of

bacterial cells on the surface of Ti samples are observed which conglomerates into

grapelike colonies, indicating the initiation of glycocalyx formation and characteristic

of biofilm [18]. In contrast, there are a few bacterial cells on Mg surface, and some of

them are found broken, suggesting that bacteria adhesion, viability and biofilm

formation is inhibited. Moreover, among the three time points, the Mg samples see the

least amount of bacterial cells at 5d, which is consistent with the results obtained by

spread plate method and CLSM.

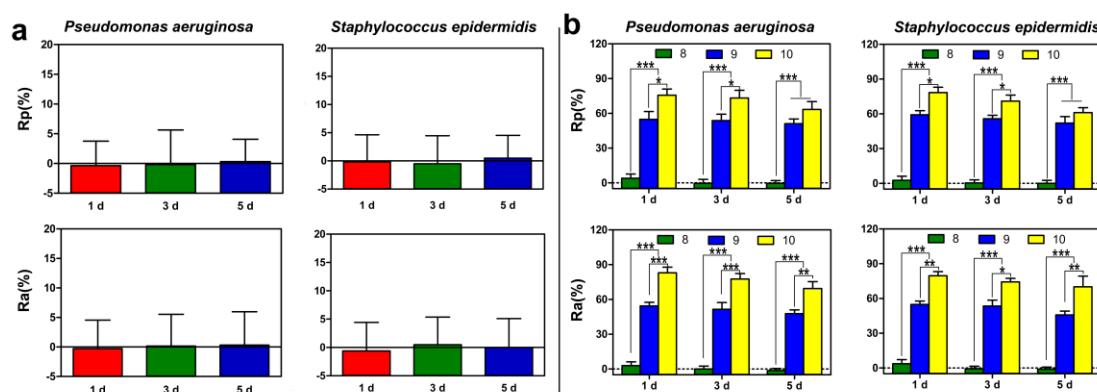## 3.4. Effect of Mg^{2+} or pH on growth of bacteria

Figure 6. Biofilm formation on Ti surface at (a) high Mg ion concentration (18mg/dl)

and (b) different pH values (8, 9, 10) examined by the spread plate method. Rp values

were used to estimate the amount of living bacteria in the medium. Ra values were

used to estimate the amount of living bacteria on Ti surface. $^*p < 0.05$, $^{**}p < 0.01$, $^{***}p < 0.001$.

As the results shown in Figure 6a, no antibacterial effect is detected when the Mg^{2+}

concentration is 18mg/dl. The effect of different pH on bacteria is shown in Figure 6b.

There is no antibacterial effect at the pH value of 8. But when pH value reaches to 9,

the Rp value is 54.9%, 53.8% and 51.1% at day 1, 3, 5 for *P. aeruginosa*, 59.2%, 55.8%

and 52.1% for *S. epidermidis*, the Ra value is 54.5%, 51.5% and 47.7% at day 1, 3, 5

for *P. aeruginosa*, 54.9%, 53.5% and 45.7% for *S. epidermidis*. With pH value rises to

10, the Rp value increases to 75.6%, 73.3% and 63.4% at day 1, 3, 5 for *P. aeruginos*a,

78.4%, 71% and 61.1% for *S. epidermidis*, the Ra value also rises to 83%, 77.6% and

69.4% for *P. aeruginosa*, 79.6%, 74.% and 70.1% for *S. epidermidis*. The Rp value of

pH 9 or pH 10 at day 1 is almost same as those of Mg corrosion in the medium at day

1 or day 3 respectively (55.1%, 74.3% at day 1, 3 for *P. aeruginosa*, 60.2%, 78.3%

for *S. epidermidis,* Figure 3a-1, 3a-2), in which pH value reaches to about 9 or 10

(Figure 2). However, the Ra value of pH 9 or pH 10 at day 1 is obviously lower than

those of Mg corrosion in the medium at day 1 or day 3 respectively (69.1%, 87.5% at

day 1, 3 for *P. aeruginosa*, 63.5%, 84% for *S. epidermidis*, Figure 3b-1, 3b-2).

3.5. *In vivo* anti-biofilm property

3.5.1. Radiographical assessment

Figure 7. Radiographical images: (A) X-rays of left femur in lateral view. Animals in group I: At 2 weeks post-op, clear signs of osteolysis and slight periosteal new bone formation emerge; At 4 weeks post-op, osteolysis and periosteal new bone formation aggravate. Animals in group II: a lot of gas appears in expanded medullary cavity and obvious periosteal new bone formation emerges at 2 weeks post-op, which exacerbate at 4 weeks post-op. Animals in groups III and IV: No signs of infection are found. White arrow, black arrow and arrowhead mark osteolysis, periosteal new bone formation, and gas respectively.

The radiographic signs of obvious osteolysis and slight periosteal reaction in all the animals of group I are evaluated by X-ray after 2 weeks. Infection develops as manifested by the exacerbation of osteolytic lesions and progress of periosteal reaction, new bone formation during the following observation time. X-ray taken

23

from group II shows lots of gas in expanded medullary cavity, obvious periosteal reaction, and a large number of new bone formation. All the X-ray images acquired from groups III and IV do not show any signs of osteolysis, periosteal reaction. (Figure 7).

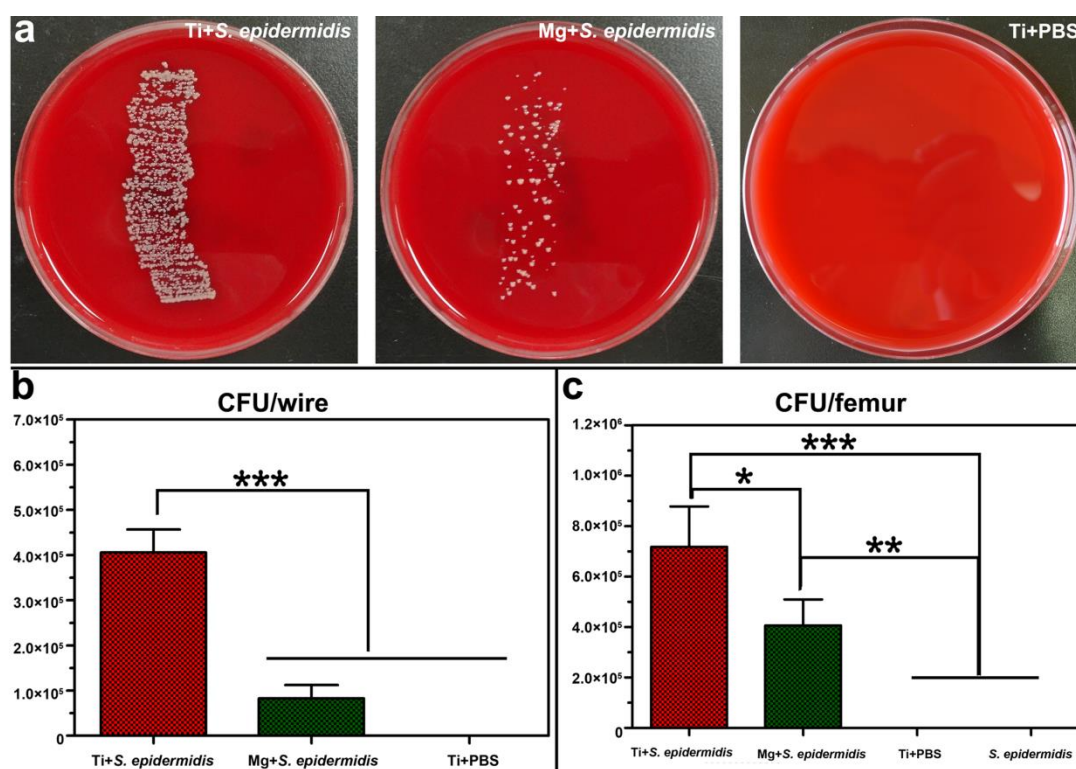### 3.5.2. Cultures of the implants

Figure 8. Cultures of implants and bone: (a) Roll-over cultures obtained from explanted Kirschner wires. (b) Counting of the dislodged adhered bacteria after wires rolling over SBA. (c) Amount of CFU per femur, quantified in pulverized bone from operated femur. $^{*}p < 0.05$, $^{**}p < 0.01$, $^{***}p < 0.001$.

All cultures of group III remain completely sterile after incubation for 24 h. The bacteria colonies detached from the wires of group I are much more than those of group II. (Figure 8a). The findings are confirmed by the results of dislodged adhered bacteria after the wires rolling over SBA showing CFUs of group I $>$ group II and no bacteria grow in group III. There are significant differences between group I and groups II, III, but no significant differences between group II and III. (Figure 8b).

3.5.3. CFU/femur

No bacteria can be cultured from the powder bones in group III and group IV. The average amount of CFU per femur of group I is found to be higher than that of group II. The differences are statistically significant among group I, group II, and groups III, IV. (Figure 8c).
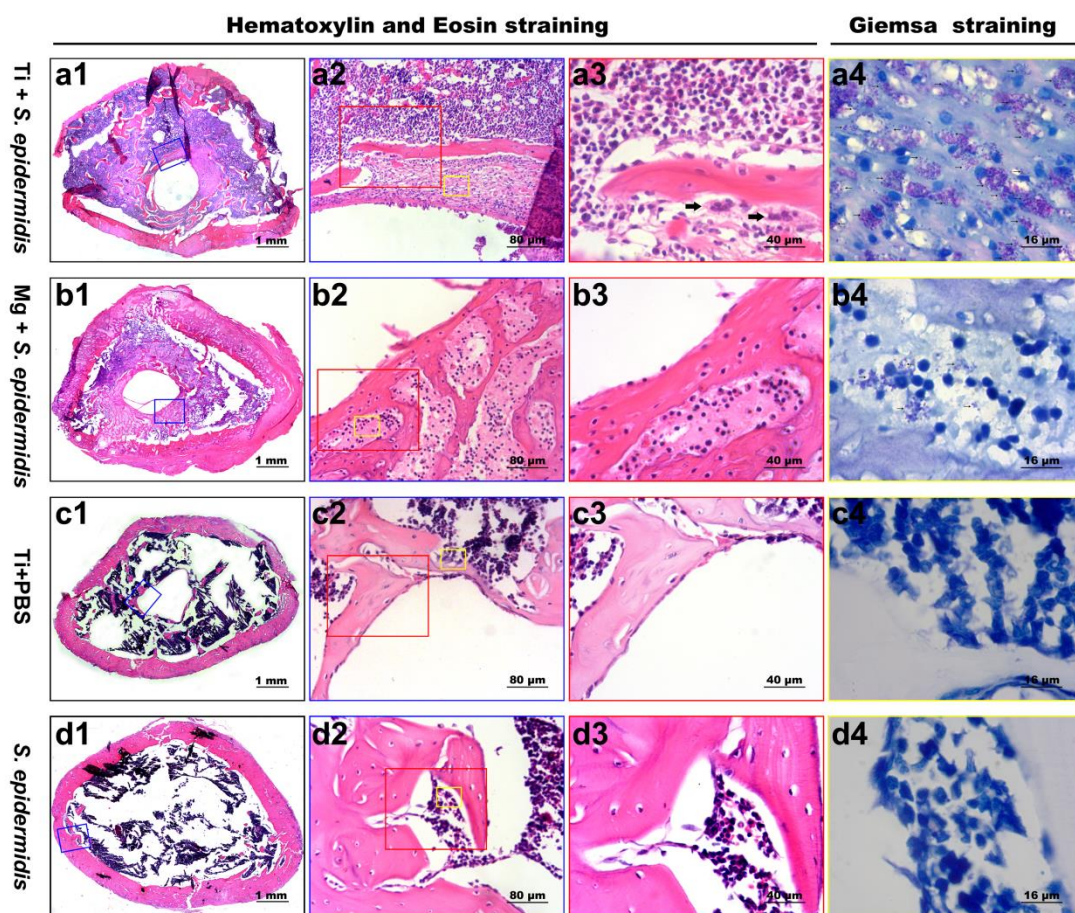
3.5.4. Histological evaluation

Figure 9. Histological slices in a transverse plane images at distal femoral cortical bone stained with Hematoxylin and eosin (HE) staining and Giemsa staining at 4 weeks after surgery. Group I: Overview image (a1) reveals massive inflammatory cells infiltrating in marrow cavity, and a layer of fibrous tissue but no direct bone formation around the Ti wire. Close-up views (a2-a3) show fibrous tissue formation at the interface of the Ti wire (a2), osteoclasts (thick arrows) invasion bone (a3) and lots of bacteria (thin arrows) persistence in the fibrous tissue (a4). Group II: Overview image (b1) displays a slight inflammatory cell infiltration, but significant proliferation of cortical bone and cancellous bone, and direct bone formation at the surface of the Mg wire. Close-up views (b2-b4) show bone formation at the interface of the Mg wire,

no osteoclasts invasion bone (b2, b3), and a very small amount of bacteria in the intramedullary tissue (b4). Group III and IV: No histopathological signs of bone infection are visible. Overview images (c1 and d1) reveal normal cells in in marrow cavity, a thin layer of bone formation at the surface of Ti wire (c1). Close-up views (c2-c4, d2-d4) show regular bone marrow without any signs of osteoclasts and bacteria. Thick arrow and thin arrow mark osteoclast and bacteria, respectively.

The morphological change on the rat femur is evaluated by HE staining, while the bacterial residue is identified using Giemsa staining. In group I, the histological slices of HE show a large number of inflammatory cells infiltration in marrow cavity, no direct bone but a layer of fibrous tissue formation at the surface of Ti wire, and the slices of Giemsa staining show that there are lots of bacteria in the intramedullary tissues, which indicate severe infections occur in the femurs of group I. In group II, there is a mild inflammatory cell infiltration, but obvious thickening of cortical bone and increase of cancellous bone, and direct bone formation at the surface of the Mg wire. The number of bacteria in the intramedullary tissues diminishes obviously. These results demonstrate that the infections in group II have been suppressed by Mg. The significant bone proliferation is related to the osteogenic effect of Mg.[19-21] In groups III and IV, neither detectable signs of infection nor bacteria can be found; a slight bone formation can be detected at the surface of Ti wire. (Figure 9).

4. Discussion

Orthopedic surgery may promote the development of implant-associated infection (IAI), which is a great challenge to the medical community and impart an immense economic burden on society [6, 22-23]. Bacteria can colonize implant surfaces and form biofilms, which is the critical step in the initiation of IAI. Once enveloped in a biofilm, bacteria become refractory to immune system and antibiotic therapy.[18, 24] Herein, we address this problem by reporting that Magnesium (Mg), a promising implant material for orthopedic applications, is protective against biofilm formed by *S. epidermidis* and *P. aeruginosa*, which are involved in IAI during orthopedic surgery.[18, 25-26]

To simulate physiological conditions, in this study, DMEM with 10% FBS is served as culture medium for bacteria. The anti-biofilm activity of Mg was assessed by three distinct techniques from two different perspectives. Microbiological counting provides a quantitative estimate to determine the number of viable bacteria in biofilm. The strength of adhesion to the implant surface will affect the efficiency of suspension of bacteria by ultrasonic vibration. Compared with the bacteria in biofilm on Ti surface, the scattered bacteria on Mg surface are easy to be detached. Consequently, comparisons of the recovered bacteria from Ti and Mg surface tend to underestimate differences. The true Ra values should be higher than the test results, which can explain why the results of CLSM and SEM seem to show the better

anti-biofilm effect. In comparison with microbiological counting, in addition to showing the number of bacteria, CLSM and SEM are more focused on the structure of the biofilm and the state of bacteria. The results consistently show that Mg is effective in inhibiting bacterial adhesion, survival and biofilm formation on its surface.

Furthermore, the anti-biofilm activity of Mg is assessed *in vivo* using a model of implant-related femur osteomyelitis in rats. According to Figures 7, 8, and 9, infection cannot be induced by injection of *S. epidermidis* (10^3 CFUs) only, but occurs in the present of a foreign implant, indicating the implant actually offers a surface for bacterial adhesion and biofilm formation, which is in accord with the clinical opinion that an implant may stimulate the onset of infection.[27] Infection in the group II cannot be judged from the radiographic images, that may be because the imaging findings of gas produced by the degradation of Mg and bone proliferation stimulated by Mg are similar to those of osteolysis and periosteal reaction caused by infection. Microbiological cultures from both the bone powder and implanted Kirschner wires and the histological results consistently show that Mg can reduce the risk of IAI.
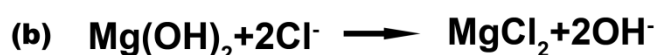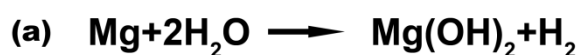
(a) $Mg + 2H_2O \longrightarrow Mg(OH)_2 + H_2$

(b) $Mg(OH)_2 + 2Cl^- \longrightarrow MgCl_2 + 2OH^-$

Figure 10. Corrosion reactions for Mg metal (a) in a pure aqueous environment and (b) in the presence of chloride ions.

How biofilm formation is inhibited on Mg sample's surface? Mg is reported to be highly unstable when in contact with water. Once contacting with water, Mg undergoes an electrochemical reaction and produces hydrogen gas (H_2) and magnesium hydroxide ($Mg(OH)_2$).[9] (Figure 10a). As Mg corrodes, the produced $Mg(OH)_2$ deposits over its surface to form a passive film to protect Mg. However, in the presence of chloride ion, $Mg(OH)_2$ can react further and produce soluble magnesium chloride ($MgCl_2$). [9, 28] (Figure 10b). Thus, Mg corrosion results in a rapid increase in Mg^{2+} concentration and pH. The higher levels of Mg^{2+} concentration and alkalinity than normal are likely to produce toxic effects on microorganisms.[14-15] To explore the mechanism responsible for the effect of Mg on biofilm, we respectively test the effect of Mg^{2+} and alkalinity on biofilm *in vitro*.

Although the excess Mg^{2+} concentration is believed to damage the enzyme and increase osmotic pressure resulting in toxic effects on microorganism,[29] Mg^{2+} at concentration of 18mg/dl has no antibacterial effect in this test. Anti-planktonic bacteria effect of the high alkalinity at pH 9 and 10 at day 1 is almost the same as that of Mg at day 1 and 3 respectively, when pH value of the solution reaches to about 9 and 10. The above results demonstrate that the antibacterial effect of Mg is ascribed to the increased alkalinity (PH$\geq$9) instead of the high Mg^{2+} concentration and is proportional to the pH value, which is consistent with the literature.[13] However, the

anti-adherent bacteria effect of the alkalinity at pH 9 and pH 10 at day 1 is obviously lower than those of Mg at day 1 and day 3 respectively. The reason may be the higher pH value on the surface of Mg than that in the solution. Because Mg corrosion happens at its surface and $Mg(OH)_2$ deposits on it, the higher pH value on Mg surface than the pH in the medium can be speculated, which is proved by Kurissery et al.[29] This can also explain why the Ra value of Mg is higher than the Rp value (Figure3). Thus, the high alkalinity at Mg surface is responsible for the effect of Mg on biofilm. In the test, the Rp and Ra values of the alkalinity at pH 9 and pH 10 decreasing with time may be associated with acidic products produced by bacterial metabolism and death which consume the hydroxyl ions and alleviate the high alkalinity.

This finding that Mg inhibits bacteria biofilm formation on its surface is significant for Mg as an implant material used in clinic. Because the milieu in the human body is a dynamic homeostatic environment, hydroxide ions generated from degradation of the Mg will be rapidly neutralized by buffer system, the alkalinity around the Mg implant *in vivo* cannot be as high as it *in vitro*,[30] the antibacterial effects against planktonic bacteria would be compromised. However, for the degradation occurred at solid-liquid interface, high alkali environment may still exist at Mg surface, so Mg may retain the anti-biofilm activity to prevent IAI, which is confirmed by our test *in vivo*.
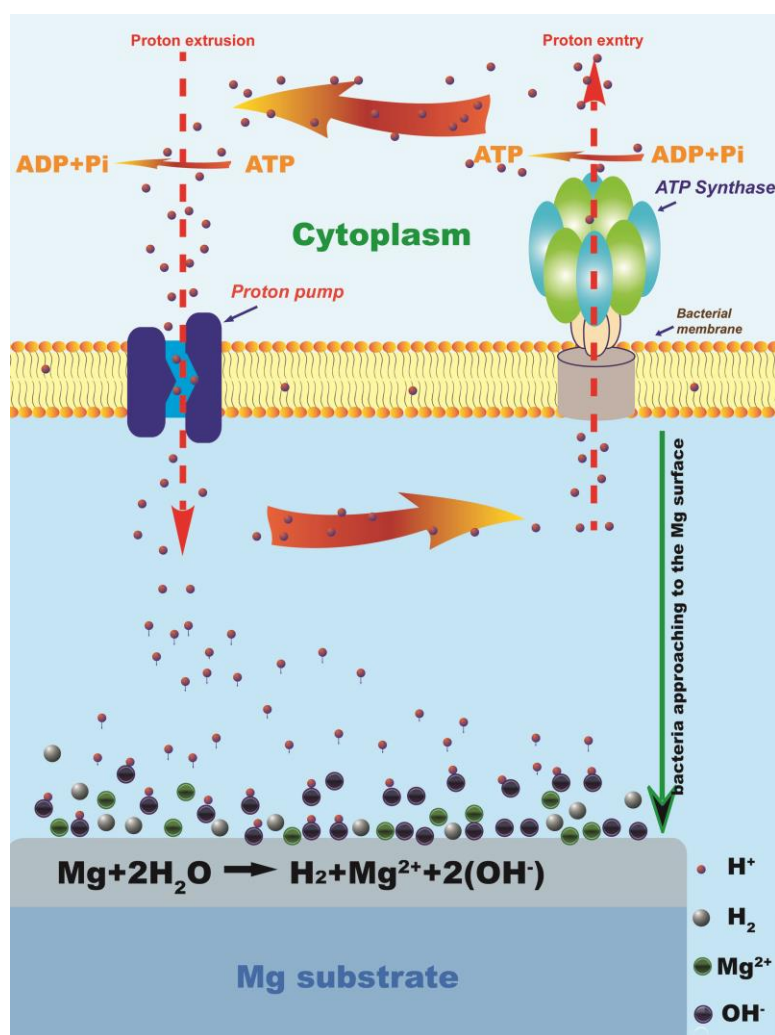
Figure 11. Illustration for the possible anti-biofilm mechanism on Mg surfaces.

How high alkalinity prevents bacterial biofilm formation? Most bacteria can only survive in an appropriate pH range (from 5.5-9).[31-32] The high alkalinity would inhibit bacterial growth,[33-34] colonization and biofilm formation.[35] It is believed that alkaline pH may impact on the chemical and/or physical bacterial surface properties and decrease bacterial surface hydrophobicity to inhibit bacteria adhesion.[35] After bacteria adhesion on the surface of Mg, a large number of H^+ produced by cell is used to neutralize the high alkalinity in overbased environment (pH≥9). Thus, the proton

electro-chemical gradient in the intermembrane space of the bacteria may be disrupted

for excessive H^+ consumption. The proton electro-chemical gradient can be

established through the net transfer of protons from the inside to the outside of the

bacteria cell by the respiration process of the electron transport chain embedded on

the cell membrane, which provide the potential energy to drive protons down the

electrochemical gradient and into the cell via the ATPase, in which protons are used

to synthesize adenosine triphosphate (ATP). Therefore, the electrochemical potential

of protons provides the driving force for the ATP synthesis.[36-38] (Figure 11). Because

ATP is the general energy source of all living cells,[39] the reduced synthesis of ATP

resulting from the interruption of the transmembrane proton electrochemical gradient

may disorder ion transport and metabolite sequestration,[40] which will interfere with

bacteria proliferation, glycocalyx synthesis, and eventually lead the bacteria death. It

is thus believed that the high alkalinity generated by Mg degradation results in the

proton depleted regions which disrupts the transmembrane proton electro-chemical

gradient and is unfavorable to bacteria survival and biofilm formation on Mg surfaces.

5. Conclusions

The anti-biofilm characteristics of Mg are studied *in vitro* and *in vivo*. Mg not only

inhibits bacterial biofilm formation *in vitro* but reduces IAI *in vivo*. Its anti-biofilm

activity is associated with high alkalinity at its surface and is independent of Mg ion.

This research offers new valuable knowledge in support of the use of Mg as a new implant material to reduce the risk of IAI.

Acknowledgment

References

1. A. G. Gristina and J. W. Costerton, *J Bone Joint Surg Am*, 1985, **67**, 264-273.

2. A. G. Gristina, M. Oga, L. X. Webb and C. D. Hobgood, *Science*, 1985, **228**, 990-993.

3. D. Campoccia, L. Montanaro and C. R. Arciola, *Biomaterials*, 2013, **34**, 8018-8029.

4. P. S. Stewart and J. W. Costerton, *Lancet*, 2001, **358**, 135-138.

5. P. Stoodley, K. Sauer, D. G. Davies and J. W. Costerton, *Annu Rev Microbiol*, 2002, **56**, 187-209.

6. R. O. Darouiche, *N Engl J Med*, 2004, **350**, 1422-1429.

7. M. van Oosten, T. Schafer, J. A. Gazendam, K. Ohlsen, E. Tsompanidou, M. C. de Goffau, H. J. Harmsen, L. M. Crane, E. Lim, K. P. Francis, L. Cheung, M. Olive, V. Ntziachristos, J. M. van Dijl and G. M. van Dam, *Nat Commun*, 2013, **4**, 2584.

8. A. D. Toms, D. Davidson, B. A. Masri and C. P. Duncan, *J Bone Joint Surg Br*, 2006, **88**, 149-155.

9. M. P. Staiger, A. M. Pietak, J. Huadmai and G. Dias, *Biomaterials*, 2006, **27**, 1728-1734.

10. N. Erdmann, N. Angrisani, J. Reifenrath, A. Lucas, F. Thorey, D. Bormann and A. Meyer-Lindenberg, *Acta Biomater*, 2011, **7**, 1421-1428.

11. T. Kraus, S. F. Fischerauer, A. C. Hanzi, P. J. Uggowitzer, J. F. Loffler and A.

M. Weinberg, *Acta Biomater*, 2012, **8**, 1230-1238.

12. Y. Shikinami and M. Okuno, *Biomaterials*, 1999, **20**, 859-877.

13. D. A. Robinson, R. W. Griffith, D. Shechtman, R. B. Evans and M. G. Conzemius, *Acta Biomater*, 2010, **6**, 1869-1877.

14. J. Y. Lock, M. Draganov, A. Whall, S. Dhillon, S. Upadhyayula, V. I. Vullev and H. Liu, *Conf Proc IEEE Eng Med Biol Soc*, 2012, **2012**, 1378-1381.

15. J. Y. Lock, E. Wyatt, S. Upadhyayula, A. Whall, V. Nunez, V. I. Vullev and H. Liu, *J Biomed Mater Res A*, 2014, **102**, 781-792.

16. Y. H. An and R. J. Friedman, *J Invest Surg*, 1998, **11**, 139-146.

17. X. Chen, D. T. Tsukayama, L. S. Kidder, C. A. Bourgeault, A. H. Schmidt and W. D. Lew, *J Orthop Res*, 2005, **23**, 816-823.

18. V. Antoci, Jr., C. S. Adams, J. Parvizi, H. M. Davidson, R. J. Composto, T. A. Freeman, E. Wickstrom, P. Ducheyne, D. Jungkind, I. M. Shapiro and N. J. Hickok, *Biomaterials*, 2008, **29**, 4684-4690.

19. F. Witte, V. Kaese, H. Haferkamp, E. Switzer, A. Meyer-Lindenberg, C. J. Wirth and H. Windhagen, *Biomaterials*, 2005, **26**, 3557-3563.

20. H. M. Wong, K. W. Yeung, K. O. Lam, V. Tam, P. K. Chu, K. D. Luk and K. M. Cheung, *Biomaterials*, 2010, **31**, 2084-2096.

21. H. M. Wong, Y. Zhao, V. Tam, S. Wu, P. K. Chu, Y. Zheng, M. K. To, F. K. Leung, K. D. Luk, K. M. Cheung and K. W. Yeung, *Biomaterials*, 2013, **34**, 9863-9876.

22. *J Bone Joint Surg Am*, 2004, **86-A**, 1328-1335.

36

23.   J. Gomez, M. Rodriguez, V. Banos, L. Martinez, M. A. Claver, J. Ruiz, E. Simarro, J. A. Canovas, M. Medina and M. Clavel, *Enferm Infecc Microbiol Clin*, 2003, **21**, 232-236.

24.   D. Campoccia, L. Montanaro, P. Speziale and C. R. Arciola, *Biomaterials*, 2010, **31**, 6363-6377.

25.   Y. Liu, Z. Zheng, J. N. Zara, C. Hsu, D. E. Soofer, K. S. Lee, R. K. Siu, L. S. Miller, X. Zhang, D. Carpenter, C. Wang, K. Ting and C. Soo, *Biomaterials*, 2012, **33**, 8745-8756.

26.   H. A. Mousa, *East Mediterr Health J*, 2001, **7**, 738-743.

27.   V. T. Andriole, D. A. Nagel and W. O. Southwick, *J Bone Joint Surg Am*, 1973, **55**, 1511-1515.

28.   G. Makar and J. Kruger, *Int Mater Rev*, 1993, **38**, 138-153.

29.   S. R. KURISSERY, N. KANAVILLIL and Y. KIKUCHI, *Trans JWRI*, 2002,**31**, 55–61.

30.   J. Walker, S. Shadanbaz, T. B. Woodfield, M. P. Staiger and G. J. Dias, *Biomed Mater*, 2014, **9**, 015006.

31.   J. L. Slonczewski, B. P. Rosen, J. R. Alger and R. M. Macnab, *Proc Natl Acad Sci U.S.A*, 1981, **78**, 6271-6275.

32.   I. R. Booth, *Microbiol Rev*, 1985, **49**, 359-378.

33.   E. Padan, E. Bibi, M. Ito and T. A. Krulwich, *Biochim Biophys Acta*, 2005, **1717**, 67-88.

34.   E. Padan, D. Zilberstein and S. Schuldiner, *Biochim Biophys Acta*, 1981, **650**,

151-166.

35. A. Nostro, L. Cellini, M. Di Giulio, M. D'Arrigo, A. Marino, A. R. Blanco, A. Favaloro, G. Cutroneo and G. Bisignano, *APMIS*, 2012, **120**, 733-742.

36. H. Cao, X. Liu, F. Meng and P. K. Chu, *Biomaterials*, 2011, **32**, 693-705.

37. P. D. Boyer, *Annu Rev Biochem*, 1997, **66**, 717-749.

38. G. Jin, H. Qin, H. Cao, S. Qian, Y. Zhao, X. Peng, X. Zhang, X. Liu and P. K. Chu, *Biomaterials*, 2014, **35**, 7699-7713.

39. C. von Ballmoos, *J Bioenerg Biomembr*, 2007, **39**, 441-445.

40. B. L. Trumpower and R. B. Gennis, *Annu Rev Biochem*, 1994, **63**, 675-716.